JOC Article

Synthesis, Dual Fluorescence, and Fluoroionophoric Behavior of Dipyridylaminomethylstilbenes

Jye-Shane Yang,*,† Yan-Duo Lin,† Ya-Ho Chang,† and Shin-Shin Wang‡

Department of Chemistry, National Central University, Chung-Li, Taiwan 32054, and Union Chemical Laboratories, Industrial Technology Research Institute, Hsinchu, Taiwan 30043

jsyang@cc.ncu.edu.tw

Received May 6, 2005

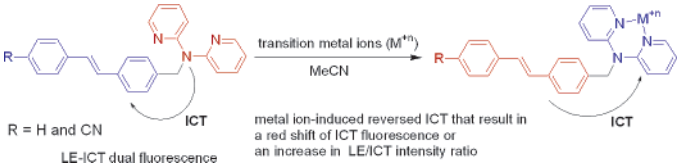

The synthesis, dual fluorescence, and fluoroionophoric behavior of two donor−σ spacer−acceptor (D-s-A) compounds, *trans*-4-(*N*,*N*-bis(2-pyridyl)amino)methylstilbene (**1H**) and *trans*-4-(*N*,*N*-bis(2-pyridyl)amino)methyl-4′-cyanostilbene (**1CN**), are reported and compared to that of *trans*-4-(*N*,*N*-bis(2-pyridyl)amino)methyl-4′-(*N*,*N*-dimethylamino)stilbene (**1DPA**). To gain insights into the dual fluorescence properties for **1H** and **1CN** in polar but not in nonpolar solvents, model compounds resulting from a replacement of the stilbene group by alkyl (**2R**) or xylyl (**2X**) groups or from a replacement of the dipyridylamino (dpa) group by dianisoleamino (**3AA**), diethylamino (**3EE**), methylanilino (**3MP**), or diphenylamino (**3PP**) groups also have been investigated. In addition to **1H** and **1CN**, all four compounds of **3** display dual fluorescence. The locally excited (LE) fluorescence mainly results from the stilbene group and the ICT fluorescence from the through-bond interactions between the amino donor and the stilbene acceptors. In the presence of transition metal ions such as Zn(II), Ni(II), Cu(II), and Cd(II), the ICT processes are switched from dpa (D) → stilbene (A) in **1H** and **1CN** to stilbene (D) → dpa/metal ion (A) in their complexes. Whereas the ICT states for the complexes are generally nonfluorescent, an exception was found for the case of **1H**/Zn(II). As a result, substituent-dependent fluoroionophoric behavior has been demonstrated by **1H**, **1CN**, and **1DPA** in response to Zn(II).

Introduction

The phenomenon of dual fluorescence emission of electron donor (D)−acceptor (A) integrated systems is attractive, because the interplay of the two emissive states with the enviroment is not only informative on excited-state D−A interactions but also useful in fluorescence sensory applications.[1−3] In general, the short- and long-wavelength fluorescence bands are ascribed to locally excited (LE) and intramolecular charge transfer (ICT) states, respectively. The highly dipolar nature of the ICT state is evidenced by a large positive solvatofluorochromism, where the fluorescence maximum shifts toward the red upon increasing solvent polarity. For donor−σ spacer−acceptor (D-s-A) systems, observations of the ICT fluorescence strongly depend on the length and flexibility of spacer and the polarity of solvent.[1,2] When the spacer allows the formation of a sandwich geometry between D and A, the ICT state could be formed in both nonpolar and polar solvents, but it is generally nonfluorescent in polar solvents such as acetonitrile, presumably due to the fast generation of well-solvated radical ion pairs ($D^{+\bullet}$-s-$A^{-\bullet}$).[1,2] The net process of D−A interactions in the latter case is thus a complete photoinduced electron transfer (PET) from D to A, corresponding to a fluorescence quenching of the LE state (D*-s-A or D-s-A*). In contrast, dual fluorescence in polar solvents has been observed for systems with short spacers such as one or two CH_2 groups.[1] While this might be an avenue toward the design of fluoroionophores with the LE-ICT

† National Central University.
‡ Industrial Technology Research Institute.

(1) Kavarnos, G. J.; Turro, N. J. *Chem. Rev.* **1986**, *86*, 401−449.
(2) Brouwer, F. In *Conformational Analysis of Molecules in Excited States*; Waluk, J., Ed.; Wiley-VCH: New York, 2000; Chapter 4, pp 177−235.
(3) (a) de Silva, A. P.; Gunaratne, H. Q. N.; Gunnlaugsson, T.; Huxley, A. J. M.; McCoy, C. P.; Rademacher, J. T.; Rice, T. E. *Chem. Rev.* **1997**, *97*, 1515−1566. (b) de Silva, A. P.; Fox, D. B.; Moody, T. S.; Weir, S. M. In *Molecular and Supramolecular Photochemistry*; Vol. 7, Optical Sensors and Switches; Marcel Deckker, Inc.; New York, 2001; pp 93−151.

10.1021/jo0509049 CCC: $30.25
Published on Web 06/24/2005

SCHEME 1

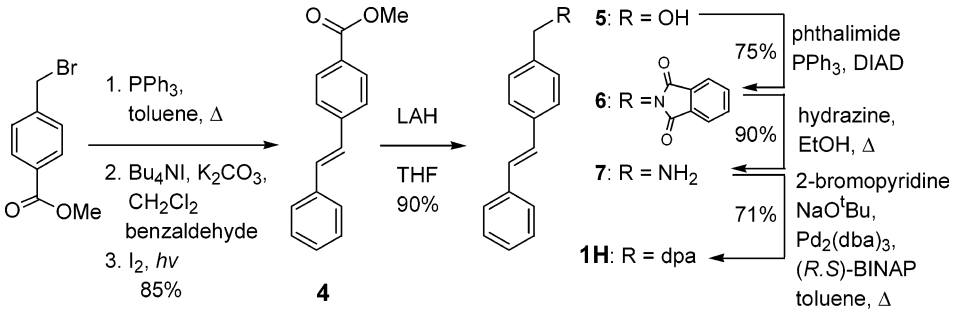

ratiometric fluorescence responses,[4,5] the vast majority of the hitherto reported ionophoric D-s-A systems, disregarding the chain length of spacers, display only the LE fluorescence and the PET-based "on−off" or "off−on" fluoroionophoric behavior in polar solvents.[3]

The *N*,*N*-bis(2-pyridyl)amino (dpa) group is known to possess a remarkable binding ability to transition metal ions such as Zn(II) and Ni(II),[6,7] which has been applied in the formation of fluoroionophores.[7,8] However, these dpa-derived D-s-A systems with a C_1 (e.g., **1DPA**) or a virtual C_0 spacer all display the "on−off"-type fluorescence sensing mode. We report herein that the dpa derivatives **1H** and **1CN** display dual fluorescence in acetonitrile, based on which the ratiometric fluorescence sensing behavior is demonstrated. In addition, the ICT fluorescence of **1H** undergoes a red shift that is selectively induced by Zn(II). To understand the dual fluorescence and fluoroionophoric properties of **1H** and **1CN**, studies on model compounds **2** and **3** were also carried out.

Results and Discussion

Synthesis and Crystal Structures. The synthetic methodology for **1H** is analogous to that previously reported for **1DPA** (Scheme 1),[8] but a different route was required for the synthesis of **1CN** (Scheme 2) due to the susceptibility of the cyano group to the LAH reduction. The intermediates **4**,[9] **5**,[10] **6**,[11] and **7**[12] in Scheme 1 are known compounds and our melting points and/or ^{1}H NMR spectra conform to the literature values. The

SCHEME 2

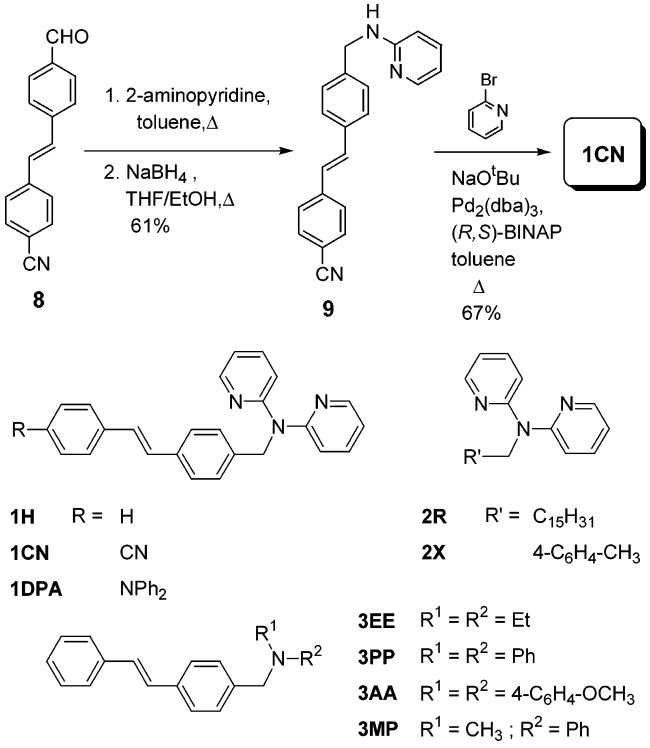

starting material **8** in Scheme 2 is also a known compound[13] and was prepared in a way similar to that for **4** with 4-cyanobenzyl bromide and 4-(diethoxymethyl)-benzaldehyde to form the stilbene backbone, followed by acid-catalyzed hydrolysis to convert the acetal to aldehyde. The conversion of **8** to **9** was via a two-step reaction, imine formation, and reduction, according to the literature procedures.[14]

Compounds **2X** and **2R**[15] were prepared following the methods in Scheme 1, starting with the Mitsunobu

(4) (a) Collins, G. E.; Choi, L.-S.; Callahan, J. H. *J. Am. Chem. Soc.* **1998**, *120*, 1474−1478. (b) Collado, D.; Perez-Inestrosa, E.; Suau, R.; Desvergne, J.-P.; Bouas-Laurent, H. *Org. Lett.* **2002**, *4*, 855−858. (c) Kawakami, J.; Kimura, H.; Nagaki, M.; Kitahara, H.; Ito, S. *J. Photochem. Photobiol. A*: *Chem.* **2004**, *161*, 141−149.

(5) (a) Sankaran, N. B.; Banthia, S.; Das, A.; Samanta, A. *New J. Chem.* **2002**, *26*, 1529−1531. (b) Boiocchi, M.; Colucci, G.; Licchelli, M.; Monzani, E.; Sacchi, D. *Chem. Commun.* **2003**, 2906−2907.

(6) (a) Ho, K.-Y.; Yu, W.-Y.; Cheung, K.-K.; Che, C.-M. *Chem. Commun.* **1998**, 2101−2102. (b) Ho, K.-Y.; Yu, W.-Y.; Cheung, K.-K.; Che, C.-M. *J. Chem. Soc., Dalton Trans.* **1999**, 1581−1586. (c) Yang, W.; Schmider, H.; Wu, Q.; Zhang, Y.-S.; Wang, S. *Inorg. Chem.* **2000**, *39*, 2397−2404. (d) Wang, S. *Coord. Chem. Rev.* **2001**, *215*, 79−98. (e) Pang, J.; Marcotte, E. J.-P.; Seward, C.; Brown, R. S.; Wang, S. *Angew. Chem., Int. Ed.* **2001**, *40*, 4042−4045. (f) Seward, C.; Pang, J.; Wang, S. *Eur. J. Inorg. Chem.* **2002**, 1390−1399. (g) Jia, W.-L.; Song, D.; Wang, S. *J. Org. Chem.* **2003**, *68*, 701−705. (h) Liu, Q.-D.; Jia, W.-L.; Wu, G.; Wang, S. *Organometallics* **2003**, *22*, 3781−3791. (i) Seward, C.; Jia, W.-L.; Wang, R.-Y.; Wang, S. *Inorg. Chem.* **2004**, *43*, 978−985.

(7) (a) Yang, J.-S.; Lin, Y.-H.; Yang, C.-S. *Org. Lett.* **2002**, *4*, 777−780. (b) Kang, Y.; Seward, C.; Song, D.; Wang, S. *Inorg. Chem.* **2003**, *42*, 2789−2797.

(8) Yang, J.-S.; Lin, Y.-D.; Lin, Y.-H.; Liao, F.-L. *J. Org. Chem.* **2004**, *69*, 3517−3525.

(9) Fuson, R. C.; Cooke, H. G., Jr. *J. Am. Chem. Soc.* **1940**, *62*, 1180−1183.

(10) Kochi, J. K.; Hammond, G. S. *J. Am. Chem. Soc.* **1953**, *75*, 3452−3458.

(11) Hadrich, D.; Berthold, F.; Steckhan, E.; Bönisch, H. *J. Med. Chem.* **1999**, *42*, 3101−3108.

(12) Cavallito, C. J.; Yun, H. S.; Edwards, M. L.; Foldes, F. F. *J. Med. Chem.* **1971**, *14*, 130−133.

(13) Erckel, R.; Frühbeis, H. *Z. Naturforsch.* **1982**, *37b*, 1472−1480.

(14) O'Connor, S. J.; Barr, K. J.; Wang, L.; Sorensen, B. K.; Tasker, A. S.; Sham, H.; Ng, S.-C.; Cohen, J.; Devine, E.; Cherian, S.; Saeed, B.; Zhang, H.; Lee, J. Y.; Warner, R.; Tahir, S.; Kovar, P.; Ewing, P.; Alder, J.; Mitten, M.; Leal, J.; Marsh, K.; Bauch, J.; Hoffman, D. J.; Sebti, S. M.; Rosenberg, S. H. *J. Med. Chem.* **1999**, *42*, 3701−3710.

(15) The choice of a long alkyl chain instead of a methyl group for **2R** is simply due to a more feasible preparation and purification.

SCHEME 3

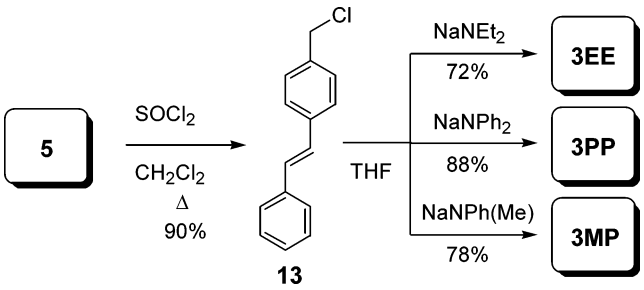

reaction[16] for 4-methylbenzyl alcohol and the Pd-catalyzed amination reaction[17] for hexadecylamine, respectively. The former was involved with known compounds **10**[18] and **11**[19] as the intermediates.

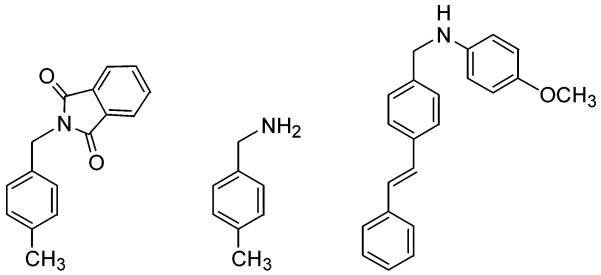

The strategies in Scheme 2 were adopted for the synthesis of **3AA** by replacing the 2-aminopyridine and 2-bromopyridine reagents with 4-methoxyaniline and 4-bromoanisole, respectively, through the intermediate **12**. However, compounds **3EE**, **3PP**, and **3MP** were prepared by S_N2 reactions between 4-chloromethylstilbene (**13**) and sodium diethylamide, sodium diphenylamide, and sodium *N*-methylanilide, respectively, where the nucleophiles were prepared in situ from sodium hydride and the corresponding amines. Compound **13** was in turn prepared from **5** by reacting with thionyl chloride.[20]

The X-ray crystal structures of **1H** and **3PP** have been determined and selected structural data are reported in Table 1.[21] For comparison, the data for **1DPA** are also included.[8] As shown in Figure 1, the stilbene group is essentially planar in both **1H** and **3PP**. Regarding the dpa group, the geometry is similar to those in the previously reported dpa derivatives in terms of the C_{py}−N bond lengths and the dihedral angles (χ_{py}) between the pyridyl planes and the plane defined by the C(sp^2)−N(amino)−C(sp^2) fragment.[6−8] In addition, as evaluated by the sum of bond angles (θ) about the amino nitrogen, the amino nitrogen atom is coplanar with the three carbon atoms to which it attaches in both cases ($\theta \sim 360°$), indicating an sp^2-hybridized character of the amino nitrogen atom. As is the case of **1DPA**, the adjacent phenyl ring of stilbene is nearly orthogonal to the CNC plane (χ_{ph}) or the pyridyl planes (χ_{ph-py}). All these values suggest that the dpa group would have a negligible orbital overlap or through-space electronic interaction with the stilbene group in **1H** and **1CN** as well as in **1DPA**.

TABLE 1. Selected Structural Data, Including the Sum of Bond Angles (θ) Around the Amino Nitrogen Atom, Dihedral Angles (χ_{ph}, χ_{py}, and χ_{ph-py}), and C_{sp2}−N Bond Lengths (d_{py}) for 1H, 1DPA, 2X, 2X/$ZnCl_2$, and 3PP

compd	θ (deg)	χ_{ph} (deg)	χ_{py} (deg)[b]	χ_{ph-py} (deg)[b]	d_{py} (Å)[b]
1H	360.0	79.2	6.2	83.5	1.390
			42.4	86.1	1.411
1DPA[a]	359.9	85.2	25.1	82.7	1.394
			37.9	84.4	1.409
2X	359.9	88.2	29.7	76.1	1.398
			30.0	84.8	1.413
2X/$ZnCl_2$	355.4	82.6	48.2	37.7	1.414
			60.9	71.7	1.410
3PP	359.8	72.1	12.5	78.9	1.389
			56.3	80.4	1.424

[a] Data from ref 8. [b] The subscript py corresponds to the pyridine ring in **1H**, **1DPA**, **2X**,and **2X**/$ZnCl_2$ and to the *N*-phenyl ring in **3PP**.

An attempt to grow single crystals of the $ZnCl_2$ complexes of compound **1H**, **1CN**, or **1DPA** was unsuccessful. However, we were able to obtain the X-ray crystal structures of **2X** and its complex with $ZnCl_2$ (**2X**/$ZnCl_2$) (Figure 1), which could serve as model compounds for compounds **1** to investigate the geometry of the dpa/$ZnCl_2$ moiety and the change in spatial alignment between the stilbene and the dpa groups upon coordination with

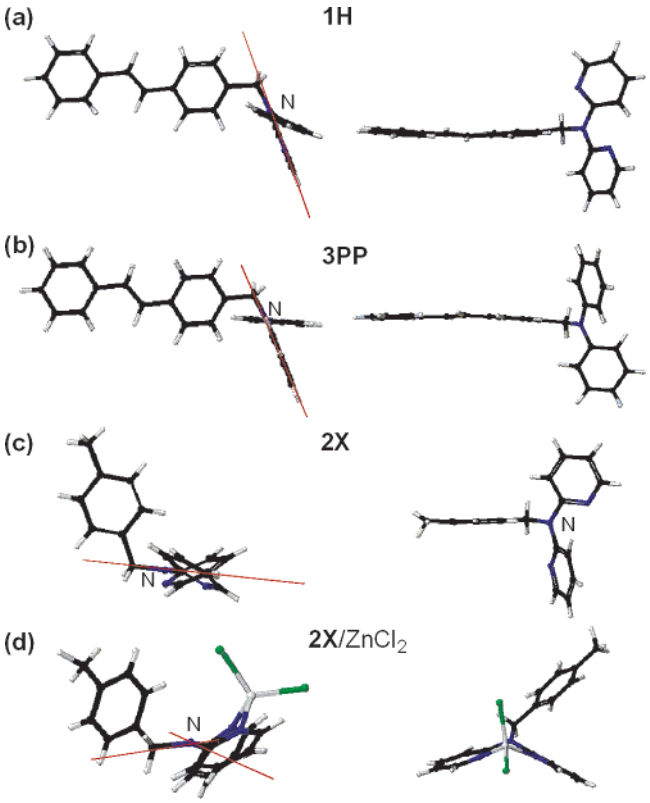

FIGURE 1. Crystal structures of (a) **1H**, (b) **3PP**, (c) **2X**, and (d) **2X**/$ZnCl_2$. The red lines highlight the planar vs pyramidal geometries of the amino nitrogen in **1H**, **3PP**, and **2X** vs **2X**/$ZnCl_2$.

(16) Mitsunobu, O. *Synthesis* **1981**, 1−28.
(17) (a) Wolfe, J. P.; Wagaw, S.; Marcoux, J.-F.; Buchwald, S. L. *Acc. Chem. Res.* **1998**, *31*, 805−818. (b) Hartwig, J. F. *Angew. Chem., Int. Ed.* **1998**, *37*, 2046−2067.
(18) Sasaki, K.; Shibata, Y.; Hashimoto, Y.; Iwasaki, S. *Biol. Pharm. Bull.* **1995**, *18*, 1228−1233.
(19) Hauser, C. R. *J. Am. Chem. Soc.* **1930**, *52*, 1108−1111.
(20) Chen, D.-W.; Beuscher, A. E., IV; Stevens, R. C.; Wirsching, P.; Lerner, R. A.; Janda, K. D. *J. Org. Chem.* **2001**, *66*, 1725−1732.
(21) See the Supporting Information for details.

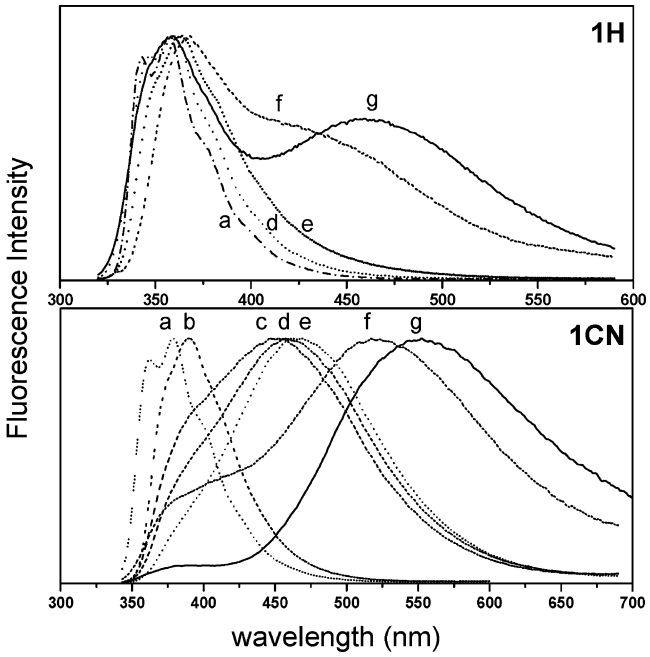

FIGURE 2. Normalized fluorescence spectra of **1H** and **1CN** in (a) hexane, (b) toluene, (c) ethyl acetate, (d) THF, (e) CH_2Cl_2, (f) acetone, and (g) MeCN. The spectra of **1H** in (b) and (c) resemble those in (a) or (d) and are not shown for the purpose of clarity.

transition metal ions. Indeed, the selected structural data for **2X** resemble those for **1H** and **1DPA** (Table 1). Thus, it is reasonable to assume that the corresponding data for their $ZnCl_2$ complexes should be similar to one another. According to the θ and χ_{py} values for **2X**/$ZnCl_2$ vs **2X**, the amino nitrogen becomes pyramidal and the C_{py}−N bond is more twisted, which indicates that the conjugation interactions in the dpa moiety, particularly between the amino lone-pair electrons and the pyridyl groups, become weaker in the complexes vs free ligands.

Photophysical Properties. As shown in Figure 2, both **1H** and **1CN** display dual fluorescence in acetonitrile (curve g). On the basis of the large solvatofluorochromic shift for the long-wavelength but not for the short-wavelength fluorescence band,[22] the short- and the long-wavelength bands can be attributed to the LE and ICT states, respectively. The ICT fluorescence could not be observed for **1H** in solvents less polar than acetone and for **1CN** in solvents less polar than ethyl acetate. Evidently, there is a larger driving force for the ICT formation in **1CN** vs **1H**, but the ICT state is thermodynamically unfavorable for both **1H** and **1CN** in nonpolar solvents. In conjunction with the larger Stokes shift ($\Delta\nu_{st}$) for the ICT fluorescence of **1CN** vs **1H** (Table 2), the D and A should correspond to the dpa and the stilbene groups, respectively. Since the crystal structures in Figure 1 reveal that the short C_1 methylene spacer in **1** cannot allow a significant orbital overlap between the D and A groups, the D−A interactions should be mainly through the σ bonds. This is also consistent with the observation of ICT fluorescence in polar but not in nonpolar solvents.[1,2,23]

(22) The slope of the plot of ICT fluorescence maxima against the solvent polarity parameter, $\Delta f = (\epsilon - 1)/(2\epsilon + 1) - 0.5(n^2 - 1)/(2n^2 + 1)$, is ~36 700 cm^{-1} for **1CN**.

TABLE 2. Maxima of UV−Vis Absorption (λ_{abs}) and Corrected Fluorescence (λ_{fl}), Stokes Shift ($\Delta\nu_{st}$), 0,0 Transition ($\lambda_{0,0}$), and Fluorescence Quantum Yields (Φ_f) for Compounds 1−3 in Acetonitrile at Room Temperature (ca. 298 K)

compd	λ_{abs} (nm)[a]	λ_{fl} (nm)	$\Delta\nu_{st}$ (cm^{-1})[b]	$\lambda_{0,0}$ (nm)[c]	Φ_f
1H	300 (311)	359, 459	5478, 11546	332	0.013
1CN	322	385, 552	5081, 12939	355	0.027
1DPA[d]	(299) 365	464	5846	415	0.68
2R	306	378	6224	338	0.045
2X	303	368	5829	335	0.035
3AA	298 (311)	358, 685	5624, 18958	329	0.002
3MP	300 (311)	356, 578	5243, 16032	332	0.021
3PP	298 (312)	359, 530	5701, 14689	332	0.013
3EE	299 (311)	359, 590	5590, 16496	332	0.003

[a] The second vibronic peak is given in parentheses. [b] $\Delta\nu_{st} = \nu_{abs}$(maximum) − ν_{fl}(maximum of the LE or ICT band). [c] The value of $\lambda_{0,0}$ was obtained from the intersection of normalized absorption and fluorescence spectra. [d] Data from ref 8.

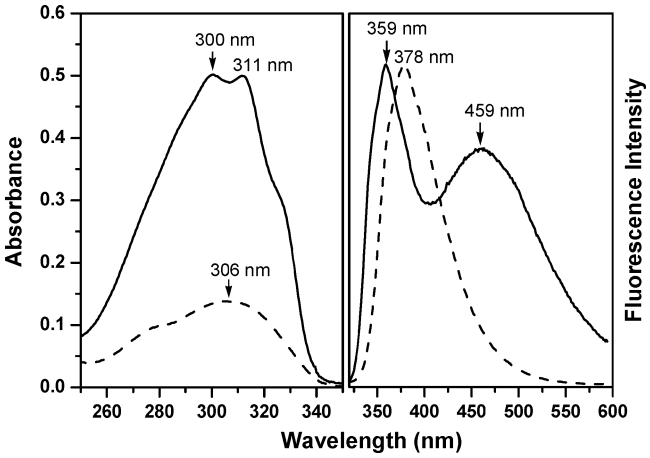

FIGURE 3. The absorption and normalized fluorescence spectra of **1H** (10 μM, solid line) and **2R** (dash line, 10 μM) in acetonitrile.

As demonstrated by **2R**, *N*-alkylated dpa compounds are fluorescent with a fluorescence quantum yield (Φ_f = 0.045, Table 2) larger than that for *trans*-stilbene (Φ_f = 0.028) and that for *trans*-4-cyanostilbene (Φ_f = 0.005)[24] in acetonitrile. However, a combination of the dpa and stilbene groups (i.e., **1H** or **1CN**) results in a weaker LE fluorescence due to the formation of an ICT state. The absorption spectrum of **2R** also overlaps very well with that of *trans*-stilbene, but the molar absorptivity (ϵ) for **2R** ($\epsilon = 1.43 \times 10^4$ L mol^{-1} cm^{-1}) is only about one-half of that for *trans*-stilbene ($\epsilon \sim 2.82 \times 10^4$ L mol^{-1} cm^{-1})[25] (Figure 3). As a result, the absorption spectrum for **1H** is more like that for *trans*-stilbene than that for **2R**. It is interesting to note that the value of ϵ (5.00×10^4 L mol^{-1} cm^{-1}) for **1H** is somewhat larger than the sum of the two components (4.25×10^4 L mol^{-1} cm^{-1}). While the

(23) (a) Hoffmann, R. *Acc. Chem. Res.* **1971**, *4*, 1−9. (b) Migita, M.; Okada, T.; Mataga, N.; Sakata, Y.; Misumi, S.; Nakashima, N.; Yoshihara, K. *Bull. Chem. Soc. Jpn.* **1981**, *54*, 3304−3311. (c) Verhoeven, J. W.; Scherer, T.; Willemse, R. J. *Pure Appl. Chem.* **1993**, *65*, 1717−1722. (d) Lewis, F. D.; Cohen, B. E. *J. Phys. Chem.* **1994**, *98*, 10591−10597. (e) Oosterbaan, W. D.; van Gerven, P. C. M.; van Walree, C. A.; Koeberg, M.; Piet, J. J.; Havenith, R. W. A.; Zwikker, J. W.; Jenneskens, L. W.; Gleiter, R. *Eur. J. Org. Chem.* **2003**, 3117−3130.
(24) Singh, A. K.; Kanvah, S. *J. Chem. Soc., Perkin Trans. 2* **2001**, 395−401.
(25) Görner, H.; Kuhn, H. J. *Adv. Photochem.* **1995**, *19*, 1−117.

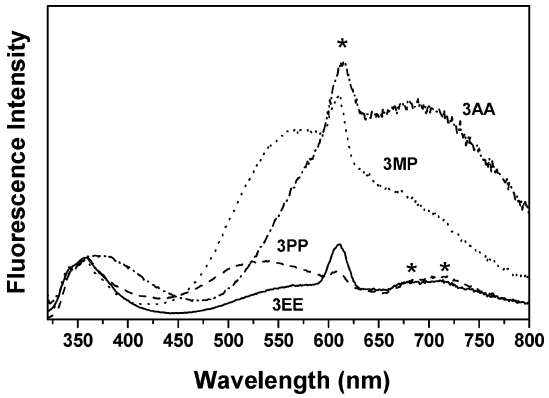

FIGURE 4. Fluorescence spectra of **3AA**, **3EE**, **3MP**, and **3PP** in acetonitrile (excitation at 310 nm). Peaks denoted with an asterisk are due to the double wavelength of the scattered light (600−620 nm) or the LE emission (660−800 nm).

excitation of **1H** should simultaneously generate two LE states, namely, D*-s-A and D-s-A*, it appears that the LE fluorescence mainly results from the stilbene fluorophore. For one reason, the fluorescence spectrum of **2R** is red-shifted by 27 nm with respect to that of *trans*-stilbene (λ_{fl} = 351 nm), but the observed LE emission (λ_{fl} = 359 nm) is stilbene-like instead of **2R**-like. In addition, compound **3EE**, which has only the stilbene fluorophore, possesses a LE band nearly the same as that of **1H** (Table 2). This in turn indicates that both the D-s-A* and D*-s-A LE states for **1H** could lead to the ICT state with the latter being more efficient. The contribution of the dpa fluorescence to the LE fluorescence of **1CN** in acetonitrile should also be low in view of its extremely weak LE band (Figure 2).

Further evidence for the dpa (D)−methylene (s)−stilbene (A) assignment in accounting for the dual fluorescence of **1H** and **1CN** is the red shift of the ICT fluorescence when the electron-donating power of the amino group is enhanced, as demonstrated by compounds **3AA**, **3EE**, **3MP**, and **3PP** (Figure 4). The driving force for the ICT state formation (ΔG_{ICT}) could be estimated according to the Weller equation:[2]

$$\Delta G_{ICT} = E_D^{ox} - E_A^{red} - E_S - 0.06\ \text{eV} \qquad (1)$$

where E_D^{ox} and E_A^{red} are the oxidation and reduction potentials of D and A, respectively, and E_S is the singlet excitation energy of D or A. The literature values[26] of E_A^{red} = −2.1 and −1.8 V (vs SCE) for *trans*-stilbene and *trans*-4-cyanostilbene, respectively, were adopted. The corresponding values of E_S were converted from the 0−0 transition energies ($\lambda_{0,0}$) of **1H** and **1CN** (Table 2). It should be noted that the values of $\lambda_{0,0}$ are essentially the same for **1H** and compounds **3**, indicating that the common stilbene group is the primary light absorber and LE-band emitter. The values of E_D^{ox} for the donors in compound series **1** and **3** could be estimated from the half-peak potentials of their cyclic voltamograms, which were recorded with respect to a reference electrode of $Ag/AgNO_3$ in dichloromethane solutions. The values of E_D^{ox} vs $Ag/AgNO_3$ were converted to the SCE electrode by addition of 0.29 V[27] or by using ferrocene ($E_{1/2}$ = 0.39 V vs SCE)[28] as an external reference. Both methods produce essentially the same results. These data along with the calculated values of ΔG_{ICT} are summarized in Table 3.

TABLE 3. Redox Potentials (E_D^{ox} and E_A^{red}),[a] Singlet Excitation Energies (E_S), and Free Energy of ICT (ΔG_{ICT}) for Compounds 1−3, 1H/Zn(II), and 1CN/Zn(II) in Acetonitrile

compd	E_D^{ox}(V)[b]	E_A^{red} (V)[b]	E_S (eV)	ΔG_{ICT} (eV)[c]
1H	1.30	−2.1[d]	3.73	−0.39
1CN	1.30	−1.8[d]	3.51	−0.47
1DPA	1.30	< −2.1	2.99	> 0.35
3AA	0.65	−2.1[d]	3.73	−1.04
3MP	0.85	−2.1[d]	3.73	−0.84
3PP	0.93	−2.1[d]	3.73	−0.76
3EE	0.96	−2.1[d]	3.73	−0.73
1H/Zn(II)	1.41[e]	−1.52[g]	3.73	−0.86
1CN/Zn(II)	1.64[f]	−1.52[g]	3.51	−0.41
1DPA/Zn(II)	0.80	−1.52[g]	2.99	−0.73

[a] Half-wave redox potentials vs SCE. [b] This work unless otherwise noted. [c] Calculated by eq 1. [d] From ref 26. [e] From ref 29. [f] From ref 30 and data converted to half-wave potential with respect to SCE. [g] Determined from **2R**/Zn(II) in dichloromethane.

It is interesting to note that for the compound series **3** the intensity ratio of the ICT/LE fluorescence maxima increases with increasing the value of $-\Delta G_{ICT}$ (i.e., **3AA** (3.37) > **3MP** (3.16) > **3PP** (0.86) > **3EE** (0.66)). The value of $-\Delta G_{ICT}$ for **1CN** is as expected to be larger than that for **1H**, but it is smaller than those for compounds **3**. However, the ICT/LE fluorescence intensity ratio for **1CN** (13.5) is the largest among the six compounds. In contrast, the corresponding dpa−stilbene interactions in **1DPA** are predicted to be thermodynamically unfavorable, which is consistent with the absence of ICT fluorescence and nearly the same fluorescence properties of **1DPA** and *trans*-*N*,*N*-diphenylaminostilbene.[8] In conjunction with their fluorescence quantum yields (Table 2), the ICT state for **1CN** appears to fluoresce the most efficiently. The correlations between the Stokes shift of ICT fluorescence and $-\Delta G_{ICT}$ are shown in Figure 5, where the six compounds could be divided into two groups with essentially the same slope. It is interesting to note that **3EE** correlates better with **1H** and **1CN** rather than with the other three compounds of **3**. In other words, with the same driving force of ICT formation (i.e., ΔG_{ICT}), the group of **1H**, **1CN**, and **3EE** are predicted to have a larger Stokes shift, corresponding to a better solvated ICT state. This appears to suggest that, in addition to the redox properties, the structural nature of the amino donor is important in determining the ICT luminescence properties of D-s-A systems.

Fluoroionophoric Behavior. Addition of Zn(II) to the acetonitrile solution of **1H** results in a shift of the ICT fluorescence toward the red from 459 to 521 nm (Figure 6a). Since the absence of a stilbene group in **2R**/Zn(II) could only lead to an emission at 479 nm, the 521-nm emission band for **1H**/Zn(II) can be ascribed to the stilbene (D)−dpa/Zn(II) (A) ICT state. In other words, a fluorescent ICT state is present in both **1H** and

(26) Léonel, E.; Paugam, J. P.; Nédélec, J.-Y.; Périchon, J. *J. Chem. Res.* (*S*) **1995**, 278−279.

(27) Suga, K.; Ohkubo, K.; Fukuzumi, S. *J. Phys. Chem. A* **2003**, *107*, 4339−4346.

(28) Zanello, P.; de Biani, F. F.; Glidewell, C.; Koenig, J.; Marsh, S. J. *Polyhedron* **1998**, *17*, 1795−1801.

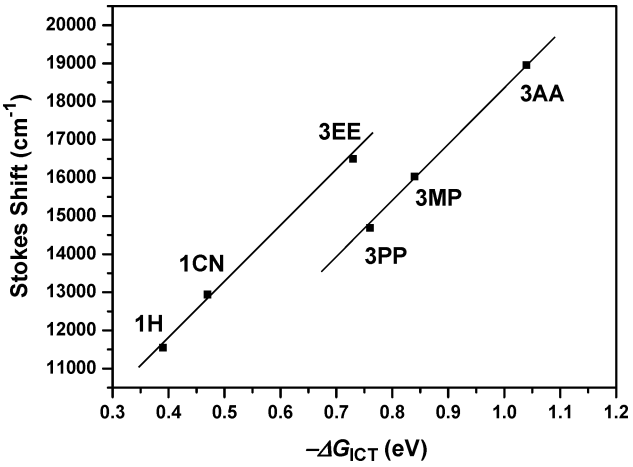

FIGURE 5. Plots of the Stokes shift of the ICT fluorescence (cm^{-1}) against the free energy of ICT formation ($-\Delta G_{ICT}$) for **1H**, **1CN**, **3AA**, **3EE**, **3MP**, and **3PP**.

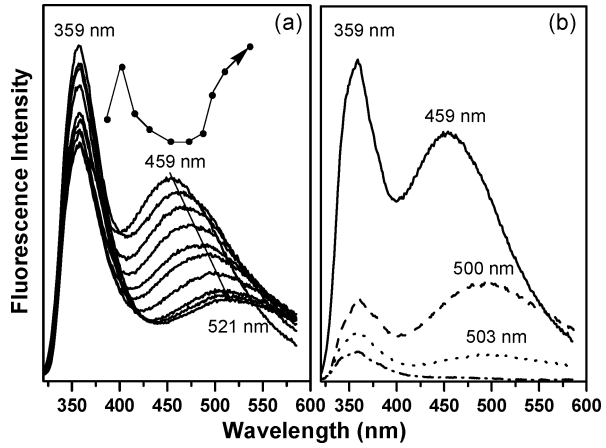

FIGURE 6. (a) Fluorescence titration spectra of **1H** (10 μM) with $Zn(ClO_4)_2 \cdot 6H_2O$ (0, 0.3, 0.4, 0.5, 0.6, 0.7, 1.0, 3.0, 5.0, 10.0 equiv) in acetonitrile (excitation at 300 nm), where the curved arrow shows the fluctuation of the LE fluorescence intensity and the arrow shows the red shift of the ICT fluorescence, and (b) fluorescence spectra of **1H** in its free form (solid line) and in the presence of a mixture of Zn(II), Ni(II), and Cd(II) (dash line, 1 equiv for each), a mixture of Zn(II), Ni(II), Cd(II), and Cu(II) (dot line, 1 equiv for each), or a mixture of Ni(II), Cd(II), and Cu(II) (dash dot line, 1 equiv for each).

1H/Zn(II), but the direction of charge transfer is reversed on going form **1H** to **1H**/Zn(II). The presence of an ICT state for **1H**/Zn(II) agrees with the electron-accepting character of dpa/Zn(II) that was previously indicated by the "on−off" fluorescence response of **1DPA** to Zn(II).[8] It is also supported by a negative value of ΔG_{ICT} calculated based on eq 1 (Table 3). According to the X-ray crystal structure of **2X**/$ZnCl_2$ (Figure 1), the stilbene−dpa/Zn(II) ICT interactions should also occur through the σ bonds. It is interesting to note that such a red-shifted ICT fluorescence is only selectively induced by Zn(II), and the other metal ions investigated in this work either quench both the ICT and the LE fluorescence (i.e., Ni(II), Hg(II), Y(III), Co(II), Cd(II), Cu(II), and Ag(I)) or have a negligible influence in the spectra (i.e., Li(I), Na(I), K(I), Mg(II), Ca(II), and Ba(II)). As shown in Figure 6b, the **1H**/Zn(II) ICT fluorescence is still observed even when the acetonitrile solution contains other transition metal ions such as Ni(II), Cd(II), and Cu(II) that are fluorescence quenchers.[31] In contrast, the LE band of **1H** does not undergo wavelength shift or monotonic intensity change upon titration with Zn(II). The fluctuation of the LE fluorescence intensity during the titration might be associated with the change in D−A character for the stilbene and dpa groups, but a more detailed mechanism remains to be investigated.

It might be interesting to make a correlation between the X-ray structures of the dpa and dpa/Zn(II) groups (Figure 1) and their ICT interactions with the stilbene group. In principle, the electron-rich amino nitrogen and the π-deficient pyridine rings in dpa and dpa/Zn(II) should dominate the electron-donating and electron-accepting character, respectively. Whereas the inductive effect of the *N*-pyridyl group would reduce the electron-donating ability of the amino nitrogen, the planar and sp^2-hybridized geometry of the amino nitrogen in free ligands in fact would facilitate the ionization process of the amino nitrogen.[32] Upon coordination with Zn(II), the electron-accepting ability of the pyridine ring would be enhanced and become sufficiently strong to interact with arenes, as previously demonstrated by the metal-ion induced fluorescence quenching or ICT formation in arene/pyridine or arene/bipyridne systems.[5,33] While the electron-accepting ability of the Zn(II)-coordinated pyridine rings in dpa/Zn(II) is expected to be reduced by the conjugated electron-donating amino nitrogen, this amino nitrogen effect appears to be largely diminished due to a pyramidylization of the amino nitrogen and a twisting of the C_{py}−N bond (i.e., less π-conjugated).

Unlike the Zn(II)-induced fluorescence quenching for **1DPA** and red shift of the ICT fluorescence for **1H**, the complexation of **1CN** with Zn(II) results in a small increase in the LE fluorescence at the large expense of the ICT fluorescence (Figure 7a). The corresponding plot of the intensity change for the ICT fluorescence against the concentration of Zn(II) is shown in Figure 7b along with the cases of Cu(II), Ni(II), and Cd(II). Nonlinear fittings of the data in Figure 7b lead to binding constants, expressed as log *K*, of 5.4, 5.1, 5.0, and 5.0 for Zn(II), Ni(II), Cu(II), and Cd(II), respectively.[34] The Weller equation (eq 1) also predicts an exogonic ICT process between the stilbene and the dpa/Zn(II) group, but the driving force is relatively smaller than that for **1H**/Zn(II) and **1DPA**/Zn(II) (Table 3). Thus, the absence of a new ICT fluorescence indicates that the ICT interaction in **1CN**/Zn(II) is weak and/or the ICT state of **1CN**/Zn(II) is nonfluorescent. In addition, the small recovery in the LE fluorescence is consistent with the inherently low fluorescence quantum yield of *trans*-4-cyanostilbene ($\Phi_f = 0.005$),[24] which is known to undergo efficient trans

(29) Majima, T.; Tojo, S.; Ishida, A.; Takamuku, S. *J. Phys. Chem.* **1996**, *100*, 13615−13623.
(30) Lewis, F. D.; Bedell, A. M.; Dykstra, R. E.; Elbert, J. E.; Gould, I. R.; Farid, S. *J. Am. Chem. Soc.* **1990**, *112*, 8055−8064.
(31) Varnes, A. W.; Dodson, R. B.; Wehry, E. L. *J. Am. Chem. Soc.* **1972**, *94*, 946−950.
(32) Sakanoue, K.; Motoda, M.; Sugimoto, M.; Sakaki, S. *J. Phys. Chem. A* **1999**, *103*, 5551−5556.
(33) (a) de Silva, A. P.; Dixon, I. M.; Gunaratne, H. Q. N.; Gunnlaugsson, T.; Maxwell, P. R. S.; Rice, T. E. *J. Am. Chem. Soc.* **1999**, *121*, 1393−1394. (b) Wagner, B. D.; McManus, G. J.; Moulton, B.; Zaworotko, M. J. *Chem. Commun.* **2002**, 2176−2177.
(34) Connors, K. A. *Binding Constants−The Measurement of Molecular Complex Stability*; John Wiley & Sons: New York, 1987; p 152.

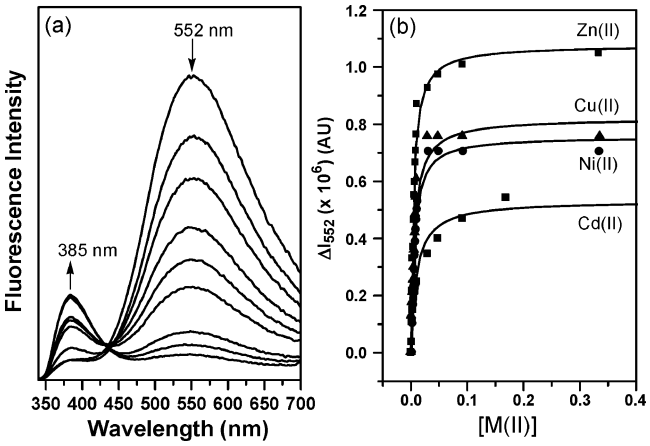

FIGURE 7. (a) Fluorescence titration spectra of **1CN** (10 μM) with $Zn(ClO_4)_2 \cdot 6H_2O$ (0, 0.2, 0.4, 0.6, 0.8, 1.0, 3.0, 5.0, 10.0 equiv) in acetonitrile (excitation at 320 nm) and (b) the corresponding plot of the change in the ICT fluorescence intensity at 552 nm (ΔI_{552}) against the concentration of Zn(II), Ni(II), Cu(II), and Cd(II).

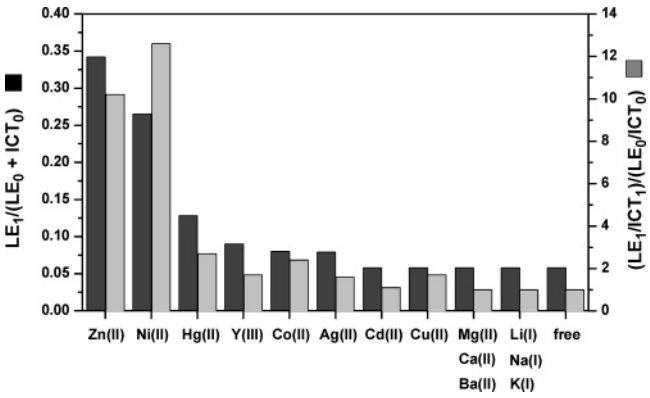

FIGURE 8. Ratiometric fluorescence responses of the LE (385 nm) vs ICT (552 nm) for **1CN** (10 μM) to 1 equiv of metal ions (10 μM) in acetonitrile.

→ cis photoisomerization.[25] Spectral changes with a decrease of the ICT band and an increase of the LE band are also observed for other transition metal ions, but the conversion yield of ICT → LE fluorescence depends on the nature of metal ions. When compared with Zn(II), the conversion yield is similar for Ni(II) but it is much smaller for metal ions such as Cu(II), Co(II), and Ag(I). Alkali and alkaline earth metal ions again show negligible effects on the fluorescence of **1CN**. These results are illustrated in Figure 8 by comparing the LE (385 nm)/ICT (552 nm) fluorescence intensity ratio (LE/ICT) at the presence of 1 equiv of metal ion vs that of the free ligand (i.e., $(LE_1/ICT_1)/(LE_0/ICT_0)$). The use of a different evaluation parameter, $LE_1/(LE_0 + ICT_0)$, focusing on the intensity of the LE band, leads to a similar result of ion selectivity.

The fluorescent ICT formation in **1H**, **1H**/Zn(II), and **1CN** is one thing particularly interesting when compared to the D-s-A systems with the dpa analogue, bis(2-pyridylmethyl)amine (dpma), as the ionophoric donor for Zn(II). The dpma derivatives display only the LE fluorescence in the absence and the presence of Zn(II) and thus the "off−on" fluorescence sensing mode.[35] For ratiometric measurement, the dpma systems require a second fluorophore[36] or the participation of fluorophore in the binding of Zn(II) (i.e., an intrinsic fluoroionophore).[37] It is noted that dpa is an arylamino donor, but dpma is an alkylamino donor. Although D−C_1 spacer−A systems with alkylamino donors generally show no ICT fluorescence, an arylamino donor is not necessary to observe dual fluorescence for current stilbene systems, as shown by **3EE**.

Concluding Remarks

The LE-ICT dual fluorescent properties for **1H** and **1CN** in acetonitrile have been investigated in the absence and presence of metal ions. The presence of ICT fluorescence in polar but not in nonpolar solvents is a characteristic of a through-bond ICT state, consistent with their short C_1 spacer. The ICT process in free ligands occurs from the dpa (D) to the stilbene (A) group. When the dpa group in **1H** is replaced by stronger amino donors, the ICT fluorescence persists with a larger Stokes shift. Upon binding with transition metal ions, the direction of ICT processes is reversed, resulting in changes in both the LE and ICT fluorescence bands. Whereas the LE/ICT intensity ratio is increased in most cases, indicating that the complexes do not produce noticeable ICT fluorescence, dual fluorescence is observed for **1H**/Zn(II). The formation of a fluorecent ICT state for **1H**/Zn(II) has provided new evidence, complementary to the Zn(II)-induced fluorescence quenching for **1DPA**, for the dpa/Zn(II) group being an effective electron acceptor. The fluorescence spectra for both the free ligands and complexes are very sensitive to the redox properties of the stilbene group, as manifested by the substituent-dependent fluoroionophoric properties for **1H**, **1CN**, and **1DPA** toward Zn(II). Our results presented herein not only show that dpa-based fluoroionophores could be selective and sensitive but also indicate that stilbene fluorophore is useful in the design of LE-ICT ratiometric D-s-A probes. Further exploration of the photochemical behavior of these and the related D-s-A systems is in progress.

Experimental Section

Materials. Solvents for organic synthesis were reagent grade or HPLC grade but all were HPLC grade for spectra and quantum yield measurements. Typical procedures for the synthesis of compounds **1**−**3** have been previously reported,[8] and the characterization data of new compounds **1H**, **1CN**, **2R**, **2X**, **3AA**, **3MP**, **3PP**, **9**, and **12** are as follows:

***trans*-4-*N*,*N*-Bis(2-pyridyl)aminomethylstilbene (1H).** Mp 118−119 °C; ^{1}H NMR (500 MHz, $CDCl_3$) δ 5.51 (s, 2H), 6.83 (dd, J = 4.9 and 7.0 Hz, 2H), 7.02 (d, J = 16.3 Hz, 1H), 7.07 (d, J = 16.3 Hz, 1H), 7.18 (d, J = 8.3 Hz, 2H), 7.24 (t, J = 7.4 Hz, 1H), 7.32−7.35 (m, 4H), 7.41 (d, J = 8.3 Hz, 2H), 7.47 (d, J = 7.4 Hz, 2H), 7.55 (ddd, J = 1.2 7.0, and 8.3 Hz, 2H), 8.31 (dd, J = 1.2 and 4.9 Hz, 2H) ppm; ^{13}C NMR (125

(35) (a) Walkup, G. K.; Burdette, S. C.; Lippard, S. J.; Tsien, R. Y. *J. Am. Chem. Soc.* **2000**, *122*, 5644−5645. (b) Hirano, T.; Kikuchi, K.; Urano, Y.; Higuchi, T.; Nagano, T. *J. Am. Chem. Soc.* **2000**, *122*, 12399−12400. (c) Burdette, S. C.; Walkup, G. K.; Spingler, B.; Tsien, R. Y.; Lippard, S. J. *J. Am. Chem. Soc.* **2001**, *123*, 7831−7841. (d) Ojida, A.; Mito-oka, Y.; Inoue, M.; Hamachi, I. *J. Am. Chem. Soc.* **2002**, *124*, 6256−6258. (e) Hirano, T.; Kikuchi, K.; Urano, Y.; Nagano, T. *J. Am. Chem. Soc.* **2002**, *124*, 6555−6562.

(36) Woodroofe, C. C.; Lippard, S. J. *J. Am. Chem. Soc.* **2003**, *125*, 11458−11459.

(37) Maruyama, S.; Kikuchi, K.; Hirano, T.; Urano, Y.; Nagano, T. *J. Am. Chem. Soc.* **2002**, *124*, 10650−10651.

MHz, $CDCl_3$) δ 51.2, 114.57, 114.60, 117.2, 126.4, 126.5, 127.5, 128.1, 128.6, 128.7, 135.8, 137.2, 137.5, 139.1, 148.3, 157.1 ppm; IR (KBr) 969, 1319, 1373, 1469 cm^{-1}; FAB-HRMS calcd for $C_{25}H_{21}N_3$ (M^+) 363.1735, found 363.1734.

***trans*-4-*N*,*N*-Bis(2-pyridyl)aminomethyl-4′-cyanostilbene (1CN).** Mp 139−141 °C; ^1H NMR (500 MHz, $CDCl_3$) δ 5.50 (s, 2H), 6.84 (dd, J = 4.9 and 7.8 Hz, 2H), 6.98 (d, J = 16.3 Hz, 1H), 7.13 (d, J = 16.3 Hz, 1H), 7.16 (d, J = 8.4 Hz, 2H), 7.35 (d, J = 8.2 Hz, 2H), 7.40 (d, J = 8.2 Hz, 2H), 7.48−7.52 (m, 4H), 7.58 (d, J = 8.4 Hz, 2H), 8.31 (dd, J = 1.4 and 4.9 Hz, 2H) ppm; ^{13}C NMR (125 MHz, $CDCl_3$) δ 51.1, 110.4, 114.5, 117.3, 119.07, 126.1, 126.8, 127.0, 127.7, 132.3, 132.5, 134.7, 137.3, 140.4, 142.0, 148.3, 157.1 ppm; IR (KBr) 963, 1322, 1468, 2218 cm^{-1}; FAB-HRMS calcd for $C_{26}H_{20}N_4$ (M^+) 388.1688, found 388.1690. Anal. Calcd for $C_{26}H_{20}N_4$: C, 80.39, H, 5.19, N, 14.42. Found: C, 80.10, H, 5.05, N, 14.43.

***N*,*N*-Bis(2-pyridyl)-*N*-hexadecylamine (2R).** Mp 36−38 °C; ^1H NMR (500 MHz, $CDCl_3$) δ 0.85 (t, J = 5.7 Hz, 3H), 1.20−1.30 (m, 26H), 1.65 (quin, J = 7.5 Hz, 2H), 4.13 (t, J = 7.5 Hz, 2H), 6.82−6.84 (m, 2H), 7.06 (d, J = 8.3 Hz, 2H), 7.48−7.51 (m, 2H), 8.33 (d, J = 4.9 Hz, 2H) ppm; ^{13}C NMR (125 MHz, $CDCl_3$) δ 14.1, 22.7, 27.1, 28.3, 29.4, 29.5, 29.6, 29.67, 29.71, 31.9, 48.4, 114.7, 116.8, 137.1, 148.3, 157.5 ppm; IR (KBr) 1321, 1376, 1468, 2847, 2917 cm^{-1}; FAB-HRMS calcd for $C_{30}H_{41}N_3$ (M^+) 395.3300, found 395.3292.

***N*,*N*-Bis(2-pyridyl)-*N*-(4-methylbenzyl)amine (2X).** Mp 98−100 °C; ^1H NMR (500 MHz, $CDCl_3$) δ 2.29 (s, 3H), 5.48 (s, 2H), 6.84 (dd, J = 4.9 and 7.2 Hz, 2H), 7.07 (d, J = 7.9 Hz, 2H), 7.18 (d, J = 8.4 Hz, 2H), 7.24 (d, J = 7.9 Hz, 2H), 7.51 (ddd, J = 1.3, 7.2 and 8.4 Hz, 4H), 8.32 (dd, J = 1.3 and 4.9 Hz, 2H) ppm; ^{13}C NMR (125 MHz, $CDCl_3$) δ 21.0, 51.0, 114.5, 117.0, 126.9, 129.0, 136.0, 136.2, 137.1, 148.2, 157.1 ppm; IR (KBr) 1227, 1375, 1426, 1470 cm^{-1}; FAB-HRMS calcd for $C_{18}H_{17}N_3$ (M^+) 275.1422, found 275.1422.

***trans*-4-*N*,*N*-Bis(4-methoxyphenyl)aminomethylstilbene (3AA).** Mp 128−129 °C; ^1H NMR (500 MHz, $CDCl_3$) δ 3.76 (s, 6H), 4.87 (s, 2H), 6.79 (d, J = 8.9 Hz, 4H), 6.95 (d, J = 8.9 Hz, 4H), 7.07 (s, 2H), 7.25 (m, 1H), 7.34 (m, 4H), 7.45 (d, J = 8.1 Hz, 2H), 7.50 (d, J = 7.5 Hz, 2H) ppm; ^{13}C(125 MHz, $CDCl_3$) δ 55.6, 56.9, 114.6, 121.8, 126.5, 126.7, 127.1, 127.5, 128.3, 128.4, 128.7, 136.0, 137.4, 142.5, 154.3 ppm; IR (KBr) 694, 965, 1238, 1514, 3386 cm^{-1}; FAB-HRMS calcd for $C_{29}H_{27}NO_2$ 421.2042, found 421.2040. Anal. Calcd for $C_{29}H_{27}NO_2$: C, 82.63, H, 6.46, N, 3.32. Found: C, 82.48, H, 6.44, N, 3.09.

***trans*-4-*N*-Methyl-*N*-phenylaminomethylstilbene (3MP).** Mp 100−101 °C; ^1H NMR (500 MHz, $CDCl_3$) δ 3.00 (s, 3H), 4.52 (s, 2H), 6.73 (m, 3H), 7.07 (s, 2H), 7.22 (m, 4H), 7.37 (t, J = 7.5 Hz, 2H), 7.44 (d, J = 8.1 Hz, 2H), 7.48 (d, J = 7.6 Hz, 2H) ppm; ^{13}C NMR (125 MHz, $CDCl_3$) δ 38.5, 56.5, 112.5, 116.6, 126.4, 126.5, 126.7, 127.2, 127.6, 128.4, 128.7, 128.9, 129.2, 136.1, 137.4, 137.5, 138.6, 149.8, 157.8 ppm; IR (KBr) 690, 960, 1221, 1258, 1495, 1589, 3024 cm^{-1}; FAB-HRMS calcd for $C_{22}H_{21}N$ 299.1674, found 299.1674.

***trans*-4-*N*,*N*-Diphenylaminomethylstilbene (3PP).** Mp 133−134 °C; ^1H NMR (500 MHz, $CDCl_3$) δ 5.00 (s, 2H), 6.93 (t, J = 7.3 Hz, 2H), 7.07 (d, J = 7.9 Hz, 6H), 7.24 (t, J = 7.2 Hz, 5H), 7.3 (m, 2H), 7.44 (d, J = 8.1 Hz, 2H), 7.49 (d, J = 7.4 Hz, 2H) ppm; ^{13}C NMR (125 MHz, $CDCl_3$) δ 56.2, 120.7, 121.4, 126.5, 126.8, 126.9, 127.6, 128.4, 128.7, 129.3, 136.0, 137.4, 138.8, 148.1 ppm; IR (KBr) 693, 962, 1221, 1258, 1495, 1589, 3024 cm^{-1}; FAB-HRMS calcd for $C_{27}H_{23}N$ 361.1830, found 361.1832.

***trans*-4-Cyano-4′-(*N*-(2-pyridyl)amino)methylstilbene (9).** Mp 199−201 °C; ^1H NMR (500 MHz, $CDCl_3$) δ 4.57 (d, J = 5.8 Hz, 2H), 5.31 (br s, 1H), 6.44 (d, J = 8.4 Hz, 1H), 6.65 (dd, J = 4.2 and 8.0 Hz, 1H), 7.10 (d, J = 16.3 Hz, 1H), 7.23 (d, J = 16.3 Hz, 1H), 7.41 (d, J = 8.1 Hz, 2H), 7.47 (dd, J = 8.0 and 8.4 Hz, 1H), 7.53 (d, J = 8.1 Hz, 2H), 7.60 (d, J = 8.3 Hz, 2H), 7.66 (d, J = 8.3 Hz, 2H), 8.13 (d, J = 4.2 Hz, 2H) ppm; ^{13}C NMR (125 MHz, $CDCl_3$) δ 46.0, 107.2, 110.6, 113.2, 119.0, 126.7, 126.8, 127.2, 127.8, 131.9, 132.5, 135.4, 138.1, 139.6, 141.8, 147.1, 158.1 ppm; IR (KBr) 969, 1325, 1472, 2218, 3243 cm^{-1}; FAB-HRMS calcd for $C_{27}H_{18}N_3$ (M + H^+) 312.1501, found 312.1495.

***trans*-4-*N*-(4-Methoxyphenyl)aminomethylstilbene (12).** Mp 153−154 °C; ^1H NMR (500 MHz, $CDCl_3$) δ 3.00 (s, 3H), 4.52 (s, 2H), 6.60 (d, J = 6.9 Hz, 2H), 6.76 (d, J = 6.9 Hz, 2H), 7.08 (s, 2H), 7.24 (m, 1H), 7.34 (m, 4H), 7.47 (d, J = 8.2 Hz, 2H), 7.50 (d, J = 8.0 Hz, 2H) ppm; ^{13}C NMR (125 MHz, $CDCl_3$) δ 49.0, 55.8, 114.2, 114.9, 126.5, 126.7, 127.6, 127.9, 128.3, 128.5, 128.7, 136.3, 137.3, 139.1, 142.3, 152.2 ppm; IR (KBr) 691, 967, 1245, 1506 cm^{-1}; FAB-HRMS calcd for $C_{22}H_{21}NO$ 315.1623, found 315.1621.

Acknowledgment. Financial support for this research was provided by the National Science Council, ROC, and by the NCU-ITRI Joint Research Center. We greatly appreciate Professor S.-L. Wang and Miss F.-L. Liao at the Instrumentation Center of National Tsing Hua University for resolving the crystal structures of **1H**, **2X**, **3PP**, and **2X**/$ZnCl_2$.

Supporting Information Available: Experimental methods, ^1H and ^{13}C NMR spectra for new compounds, and crystal refinement data for **1H**, **2X**, **3PP**, and **2X**/$ZnCl_2$, as well as X-ray experimental details (CIF). This material is available free of charge via the Internet at http://pubs.acs.org.

JO0509049